ChemCatChem

ChemCatChem
Chemistry Europe
European Chemical Societies Publishing

RESEARCH ARTICLE OPEN ACCESS

Modeling and Simulation of Combined CO_2 Capture and Hydrogenation to Methanol at Atmospheric Pressure and Low Temperature

Sofia Angeli[2] | Huidong Xu[3] | Tobias Beger[4] | Juliane Titus-Emse[4] | Andreas Jentys[3] | Roger Gläser[4] | Olaf Deutschmann[1,2]

[1]Institute for Chemical Technology and Polymer Chemistry, Karlsruhe Institute of Technology, Karlsruhe, Germany | [2]Institute of Catalysis Research and Technology, Karlsruhe Institute of Technology, Eggenstein-Leopoldshafen, Germany | [3]School of Natural Sciences, and Catalysis Research Center, Institute for Industrial Chemistry and Heterogeneous Catalysis, Technical University of Munich, Garching, Germany | [4]Institute of Chemical Technology, Leipzig University, Leipzig, Germany

Correspondence: Andreas Jentys (jentys@tum.de) | Roger Gläser (roger.glaeser@uni-leipzig.de) | Olaf Deutschmann (deutschmann@kit.edu)

Received: 27 August 2025 | **Revised:** 10 December 2025 | **Accepted:** 15 December 2025

Keywords: bifunctional catalyst | CCU | CO_2 capture | CO_2 hydrogenation | OMP

ABSTRACT

Carbon capture and utilization play an important role by converting CO_2 emissions to high value fuels and chemicals such as methanol. This work reports the modelling and simulation of the CCU to methanol using a bifunctional catalyst with amine sites for CO_2 capture and Pt sites to catalyze the reduction of intermediates to methanol. The bifunctional material exhibited high CO_2 capture capacity under post-combustion conditions at 50°C–70°C and promising methanol formation under dynamic experiments of sequential CO_2 capture and hydrogenation steps. CO_2 sorption experiments using TGA were employed to extract kinetics for the CO_2 capture. Steady-state CO_2 hydrogenation over the bifunctional material was used for the development of the hydrogenation kinetic model. The validation of the kinetic models coupled with a transient reactor model under dynamic conditions showed that the model can predict the transient formation of methanol. A parametric investigation under varying operation conditions highlighted the advantage of isothermal cycles at high temperature with respect to experimental time efficiency and maximized methanol formation rate compromised by the lower capture capacity. Further investigations in material development focusing on the facilitation of the methanol desorption from the pores would significantly improve the combined process and allow more time-efficient screening protocols.

1 | Introduction

Carbon capture and utilization (CCU) involve capturing CO_2 emissions from industrial processes and utilizing them to produce valuable products. This concept not only reduces anthropogenic CO_2 emissions but also provides a sustainable feedstock for chemical production [1]. Among various products that can be synthesized from CO_2, methanol is of high interest because it can be used as a hydrogen carrier or directly as fuel. In addition, methanol is used as a fundamental chemical building block in the production of chemicals such as formaldehyde and acetic acid [2].

The conventional methanol production process is based on the conversion of syngas, usually generated from natural gas, to methanol under a pressure of 50–100 bar and in a temperature range of 200°C–300°C [3]. The CO_2 hydrogenation process consists of two reactions: methanol formation which is exothermic, and the reverse water-gas-shift reaction, which is considered as an

undesired reaction because it also consumes hydrogen and lowers the yield of methanol production. In the absence of CO, methanol synthesis can proceed via CO_2 hydrogenation through R1. The main process comprises the formation of CO and water via reverse water gas shift reaction (RWGS) as in R2 and hydrogenation of CO as in R3.

$$CO_2 + 3H_2 \rightleftharpoons CH_3OH + H_2O \quad \text{(R1)}$$

$$CO_2 + H_2 \rightleftharpoons CO + H_2O \quad \text{(R2)}$$

$$CO + 2H_2 \rightleftharpoons CH_3OH \quad \text{(R3)}$$

Currently, commercial low-pressure catalysts generally are based on CuO and ZnO supported on Al_2O_3 with variable stabilizing additives and promoters [3, 4]. While the CO_2-based process is industrially realized, there are still challenges to overcome such as the thermodynamic limitation at a high temperature where reaction kinetics are faster and the competition with the RWGS reaction. To overcome these limitations, liquid-phase and solvent-assisted processes have been proposed as well as alternative reactor designs such as membrane reactors [5].

Within the CCU concept, alternative integrated processes of CO_2 capture and in situ conversion to methanol either in amine solutions or over amine-based solid materials as the capturing agent offer the advantage of intensified processes to instantly convert the captured CO_2 and store it chemically within the methanol molecules [6–9]. The desired properties of these materials include fast CO_2 capture kinetics, favored interaction of the captured CO_2 with the catalytic site and stability of the performance under multi-cyclic operation [10]. The immobilization of the amine functional groups on solid materials instead of a solution-based process was proven beneficial for the regeneration of the amines and the sustainability of the process [11]. Long chain polyamines were found to increase the density of the amine sites, not only advancing the CO_2 capture [12] but also the structural morphology of the material. The stabilization of carbamate species to capture CO_2 has been identified to be of utmost importance [6], but the mechanism toward the formation and selectivity to methanol is strongly dependent on additives [13, 14] as well as the morphology and the nature of the materials [12, 15]. In our previous studies, we developed bifunctional basic-metallic catalysts with 25% conversion of captured CO_2 to methanol [16, 17]. We showed that Pd-amine functionalized silica can capture and selectively convert CO_2 to methanol. The reaction proceeds via carbamate formation upon reaction of two amines with one CO_2 molecule [18]. The availability of amine sites along the metal-amine interphase is crucial in order to optimize the conversion of captured CO_2 to methanol. This can also be achieved by decreasing the pore size, where the 3D configuration of the sites in the pores leads to improved proximity of amine sites to the metal beyond the interface [17].

Ordered mesoporous polymers (OMP) with well-defined channels are good candidates for such applications, due to their large surface area, controlled and uniform pore structure, chemically inert nature, and mechanical stability [19]. Reports on nitrogen-doped mesoporous polymeric materials are primarily focused on CO_2 capture and separation [20, 21]. In our previous work, we first reported the one-step synthesis of primary amine-functionalized OMP for integrated CO_2-to-methanol conversion, demonstrating their dual functionality in CCU. In a fixed bed reactor filled with Pt/O-NOMP as catalyst, 40% of irreversibly adsorbed CO_2 (0.202 mmol g^{-1} $cycle^{-1}$) was converted to methanol with almost 100% selectivity (80 μmol g^{-1} $cycle^{-1}$) when the temperature was increased from 70°C to 120°C [22]. Furthermore, the protonation of primary amines in aqueous environments guide the loading of Pt^{IV} ions near amine groups via electrostatic attraction, which has led to substantial improvement of the catalytic performance [22].

While the material properties define the maximum CO_2 capture capacity and the pathway toward methanol, the reaction conditions are critical as well. An optimum temperature is required to maximize capture performance and reduce the amount of CO_2 being desorbed without reaction, thus enhancing the methanol yield. Kinetic modeling and simulations provide the way to optimized conditions for maximum efficiency and aid in the design and development of processes. To the best of our knowledge, there is yet no report on kinetic simulations of the integrated CO_2 capture and conversion to methanol using amine-Pt bifunctional materials. In this work, a lumped kinetic model is developed that describes the CO_2 capture and conversion processes and allows the prediction of the performance of the bifunctional material under dynamic conditions. A simulation investigation explores the effect of operation conditions on methanol formation with view of the optimization of the material testing protocols that will accelerate the screening of the materials.

2 | Experimental Section

2.1 | Material Preparation

The one-step synthesis of the ordered mesoporous polymer (OMP) followed the self-assembly route using Pluronic F127 as a soft template. Typically, 2.2 g of Pluronic F127, 1.1 g resorcinol (R), 0.7 g of hexamethylentetramin (HMT), and 2.0 mL of aqueous ammonia (28 wt.%) were mixed with 54 mL of deionized water. Once all reactants were dissolved, 0.35 g of HMT was additionally added. The reactant molar ratio of F127: R: HMT: NH_3: H_2O was 0.0175: 1: 1.75: 2.7: 311. A dark blue solution was obtained, which was stirred for 48 h at 80°C until reddish solid products were formed and cooled to room temperature, collected by filtration, washed with distilled water, and dried in air at 80°C. Finally, the solid was calcined in a tubular furnace at 350°C for 3 h, with a heating rate of 1°C min^{-1} under a flow of N_2 (100 mL min^{-1}). After calcination, the material was denoted as O-OMP.

The addition of the primary amine on the O-OMP was carried out using 3-(3-aminopropyl)phenol (APP) as an amine source via a similar route. The molar ratio of F127: R: APP: HMT: NH_3: H_2O was 0.0175: 0.7: 0.3: 1.75: 2.6: 311. Other steps remained the same as in the synthesis of O-OMP. After calcination, the material was denoted as O-NOMP.

The loading of the O-NOMP sorbent with platinum was realized via the evaporation-induced self-assembly (EISA) method. 1 g NOMP was stirred in a 0.01 M aqueous H_2PtCl_6 solution (55 mL for designated Pt loading of 4 wt.%) at room temperature for

6 h. Subsequent reduction of Pt^{IV} to $Pt^{(0}$ was carried out with 0.1 M aqueous $NaBH_4$ solution used in excess. The materials were dried at 80°C overnight, and the samples were designated as Pt/O-NOMP.

2.2 | Characterization

The carbon, hydrogen, and nitrogen content of the bifunctional catalyst was determined using a HEKAtech Euro EA Elemental Analyzer. The samples were oxidized at 1800°C and the combustion gases were chromatographically separated and detected using a TCD detector. Atomic absorption spectroscopy (AAS) was used to determine the Pt-content using a Solaar M5 Dual Flame graphite furnace AAS spectrometer from ThermoFisher. For analysis, 50–80 mg of the sample was dissolved in hydrofluoric acid, which was subsequently evaporated. The solid residue was dissolved in sulfuric acid and analyzed.

The average particle size of Pt was measured by transmission electron microscopy. The catalyst sample was dispersed in ethanol and drops of the catalyst suspensions were applied on a 400-mesh copper grid. The measurements were carried out in a JEOL JEM-1470plus electron microscope with an accelerating voltage of 120 keV. Statistical size analysis of the metal particle size was obtained using at least 100 particles from representative transmission electron microscopy micrographs.

The BET-surface area was determined by N_2-physisorption at −196°C in an automated nitrogen adsorption analyzer Sorptomatic 1990 Series (Thermo Fisher). Prior to adsorption, the samples were outgassed in vacuum at 160°C for 4 h.

2.3 | CO_2 Capture Performance

The capture capacity of the sorbent was evaluated using thermogravimetric analysis (TGA). The CO_2 adsorption measurements were carried out at ambient pressure and under flow conditions in a Setaram SENSYS Evo TG-DSC. Before the experiments, the samples were pretreated for 2 h at 120°C in 150 mL·min^{-1} of N_2. The adsorption was studied at 30°C, 50°C, and 70°C in a stream of diluted CO_2 in N_2 (3-10 vol.% CO_2, with a total flow of 112 mL min^{-1}) for 3 h, followed by purging with N_2 (150 mL min^{-1}) for 2 h at the same temperature. Desorption of CO_2 was carried out by heating to 90°C at a rate of 3°C min^{-1} under 150 mL min^{-1} N_2. The equilibrium CO_2 uptake, q_e, was calculated based on the mass increase during the adsorption step.

$$q_e = \frac{m_{eq.} - m_{sample}}{M_{CO_2} \times m_{sample}} \quad (1)$$

where m_{sample} is the sample mass at the start of the adsorption step.

The chemisorbed amount of CO_2 was determined based on the mass loss during the purging process with high flow N_2 and calculated as

$$q_{chem} = \frac{m_{purge} - m_{sample}}{M_{CO_2} \times m_{sample}} \quad (2)$$

where m_{sample} is the mass of the sample measured by the TGA at $t = 0$ for each cycle and M_{CO_2} is the molar mass of CO_2.

2.4 | Steady-State Methanol Synthesis

Steady-state CO_2 hydrogenation experiments were carried out to evaluate the steady state kinetics of the bifunctional catalyst. The activity was measured using a fixed-bed tubular reactor at 1 bar and temperatures between 70°C and 160°C. Before starting the reaction, the catalyst was pre-treated in N_2 (100 mL min^{-1}) at 140°C for 2 h and subsequently reduced in 30 vol.% H_2 (balance He) at 140°C for 1 h under a total flow of 44 mL min^{-1}. After cooling down to 70°C in N_2 atmosphere the CO_2 hydrogenation was studied using a gaseous composition of 3.3 vol.-% CO_2, 10 vol.% H_2, 37 vol.% He, balance N_2 with a total flow rate of 130 mL min^{-1}. After reaching steady state, the reaction temperature was changed to the next test state under reaction gas flow. The composition of the outlet gas was analyzed using an OmniStar GSD320 mass spectrometer in a m/z range between 2 and 50 to include the typical side products of this reaction (e.g., CO, CH_4, CH_2O, HCOOH, and CH_3CH_2OH). A calibration was performed for H_2, CO_2, CH_3OH, and H_2O using He as the internal standard for the quantitative evaluation of the mass spectra.

2.5 | CO_2 Hydrogenation to Methanol Under Dynamic Operation

The catalytic activity was measured using a fixed-bed tubular reactor at 1 bar and temperatures between 70°C and 120°C, applying dynamic changes in the reactant feed in order to simulate the periodic operation of a CO_2 absorber followed by reactive regeneration. Before starting the reaction cycles, 0.25 g of the bifunctional catalyst was treated in N_2 flow (100 mL min^{-1}) at 140°C for 2 h and reduced in 30 vol.% H_2 balance He at 140°C for 1 h (total flow rate 44 mL min^{-1}). The experimental procedure consists of the CO_2 capture with 10 vol.% CO_2 in He at 70°C (total flow rate 27 mL min^{-1}) for 1 h as the first step. Between the CO_2 capture and the subsequent hydrogenation step, the system was flushed with a flow of 100 mL min^{-1} N_2 for 8 min. The hydrogenation was carried out using a gas stream of 30 vol.% H_2 balanced in He (total flow 44 mL min^{-1}) while increasing the temperature (linear temperature increase 2.5 K min^{-1}) from 70°C to 120°C. The species formed during the reaction were analyzed by mass spectrometry as described for the steady-state hydrogenation experiments.

2.6 | Modeling

In order to simulate the integrated CO_2 capture and hydrogenation to methanol over the bifunctional catalyst Pt-O-NOMP, the kinetics of the sub-processes were separately investigated. The kinetics of CO_2 capture were extracted from experimental TGA measurements at the temperature of 30°C, 50°C, and 70°C and varying CO_2 inlet concentrations. The adsorption/desorption kinetics were fitted to the temperature-programmed desorption profiles of CO_2 obtained after adsorption at different temperatures as well as to the overall amount of chemisorbed CO_2 determined at the corresponding temperature. The adsorption profiles were

not considered for fitting the kinetic model due to high noise-to-signal ratio.

The experimental investigation on the low-temperature CO_2 hydrogenation to methanol was used to extract the apparent kinetic coefficients of the methanol formation reaction. Subsequently, validation of the kinetic model developed was realized by simulating the methanol formation under dynamic conditions. The validated model was then applied to run a simulation investigation under varying conditions and operational scenarios.

2.7 | Chemical Model

The capture of CO_2 over amine-based materials have been found to proceed via a proton exchange between two amine groups, as one amine group acts as a nucleophile to attract CO_2, while the other acts as a Brønsted base [23–25]. The lumped kinetic model developed considers a global, reversible surface reaction of gaseous CO_2 with the amine sites, here denoted as "s," toward adsorbed CO_2.

$$CO_2\,(g) + 2s \rightleftharpoons CO_2\,(ads) + s \tag{R4}$$

The number of available active sites (surface site density) was estimated based on the nitrogen content determined by the elemental analysis of the sample and the specific surface area determined by BET:

$$\Gamma = \frac{\frac{\omega_N}{100}\frac{m}{A_N}}{a_{s,\,BET}} \tag{3}$$

where ω_N is the nitrogen content, m is the sample mass used in the experiment, A_N is the atomic mass of nitrogen, and $a_{s,\,BET}$ is the specific surface area. The resulting surface site density for the amine sites was calculated as 3.86 10^{-6} mol m^{-2}.

The surface reaction rate $\dot{s}_i$ of the surface species i was modeled as

$$\dot{s}_i = k_{f,k}\prod_{i=1}^{N_g+N_s} c_j^{\upsilon'_{ik}} - k_{r,k}\prod_{i=1}^{N_g+N_s} c_j^{\upsilon''_{ik}} \tag{4}$$

where the rate coefficients follow an Arrhenius-type expression:

$$k_k = A_k T^{\beta_k}\exp\left[-\frac{E_{a,k}}{RT}\right] \tag{5}$$

where k_k is the rate coefficient in the step k for the given reaction, $E_{a,k}$ the activation energy, A_k the pre-exponential factor, β a fitting parameter regarding the temperature dependency of the pre-exponential factor, and R the universal gas constant. The rates are calculated under the assumption that the surface sites are uniformly distributed (mean-field approximation).

The mechanism of methanol formation from CO_2 captured over amine-loaded materials proceeds via the formation of carbamate to N-formyl intermediates to methanol [6, 8]. The role of the metal in the mechanism is to provide the catalytic cycle with dissociated hydrogen. The kinetics of CO_2 hydrogenation toward methanol over the bifunctional material was modeled considering the global reaction R1. The apparent kinetic coefficients were determined by linear fitting of the Arrhenius equation to the steady-state kinetic experiments at the temperature range of 70°C–120°C.

$$\ln(k) = \ln(A) - \frac{E_\alpha}{R}\frac{1}{T} \tag{6}$$

where k the kinetic constant, A the preexponential factor, E_a the activation energy, and R the universal gas constant.

For the simulation of the combined process of CO_2 capture and conversion to methanol, both the reactions R1 and R4 are considered with the kinetic coefficients determined as described above. In this case, the surface site density of Pt, Γ_{Pt} , was 2.72 10^{-5} mol m^{-2}.

TABLE 1 | Model parameters for the simulations of the TGA experiments with a packed bed reactor model.

Reactor ID (m)	0.005
Bed length (m)	3.16 10^{-3}
Bed porosity (−)	0.4
$F_{cat/geo}$ [a]	55794
Inlet gas velocity—adsorption step (m s^{-1})	0.093 (@25°C)
Inlet gas velocity—flushing/desorption step (m s^{-1})	0.124 (@25°C)

[a]Ratio of catalytic to geometric area of the reactor. Catalytic area, A_{cat} in this case is the amine functional groups that are considered to be evenly distributed over the whole surface area of the sample: $A_{cat} = S_{BET\times}m$. Geometric area of the reactor is the surface of the sample particles.

2.8 | Reactor Model

The kinetics of the CO_2 captured were determined adjusting the kinetic coefficients of R4 to better describe the TGA profiles. In the TGA configuration, the gas flow is inserted via a vertical tube with an internal diameter of 8 mm toward the crucible of internal diameter of 5 mm where the sample is placed. Due to the low sample mass loaded during the experiments, the resulting height of the packed bed is ca. 3 mm, allowing the assumption of a fixed bed reactor. The linear velocity of the inlet gas was calculated considering the flow through the inlet tube. The model parameters of the TGA experiments are presented in Table 1.

The simulations were carried out using the DETCHEM^{PBR_TRANSIENT} simulation package. This is a 1D fixed-bed reactor model, which assumes no radial variations in flow properties as well as negligible axial diffusion compared to the convective terms [26]. The governing equations include the continuity (Equation 7) and the gas phase species balances (Equation 8):

$$\frac{d(\rho u)}{dz} = a_v\sum_{i\epsilon S_g} M_i\dot{s}_i \tag{7}$$

TABLE 2 | Model parameters for modeling of the internal diffusion.

Average particle size (m)	$303\ 10^{-6}$
Pore size (m)	$4.98\ 10^{-9}$
Pore Volume ($cm^3\ g^{-1}$)	0.78
Particle porosity	0.104
Tortuosity	3

$$\rho u \frac{dY_i}{dz} + Y_i a_v \sum_{i \epsilon S_g} M_i \dot{s}_i = M_i \left(a_v \dot{s}_i + \dot{\omega}_i \varepsilon \right) \tag{8}$$

where ρ is the fluid phase density, z the axial coordinate of the reactor, u the superficial velocity, a_v the total particle surface area to catalytic bed volume ratio, $\dot{s}_i$ the surface phase reaction rate, M_i the molar mass of species i, Y_i the mass fraction of gas phase species i, $\dot{\omega}_i$ the gas phase reaction rate, and ε the catalytic bed porosity.

Internal diffusion of CO_2 might become important since it must diffuse into the pores of the material to reach further active sites, resulting in concentration gradients. The pore diffusion was modeled using an effectiveness factor, which is the ratio of the surface reaction rate under diffusion limitations by the surface rate in the absence of diffusion limitations (spherical particles assumed).

$$\eta_i = \frac{\overline{\dot{s}_i}}{\dot{s}_i} = \frac{3}{\varphi^2} \{\varphi [\coth \varphi] - 1\} \tag{9}$$

$$\varphi = L \sqrt{\frac{k}{D_{eff,i}}} \tag{10}$$

where φ is the Thiele modulus, $D_{eff,i}$ is the mixed diffusion coefficient, and k the reaction rate coefficient.

The mixed diffusion coefficient is calculated from contributions from both molecular and Knudsen diffusion as follows:

$$D_{eff,\,i} = \frac{\epsilon_p}{\tau} \overline{D_i} \tag{11}$$

$$\overline{D_i} = \frac{1}{D_{mol,\,i}} + \frac{1}{D_{knud,\,i}} \tag{12}$$

where ε_p is the particle porosity, τ is the tortuosity, $D_{mol,\,i}$ is the molecular diffusion coefficient, and $D_{knud,\,i}$ is the Knudsen diffusion coefficient. The model parameters for the internal diffusion model are summarized in Table 2.

The mass transfer resistance from the surface to the bulk of the gas phase was also included in the model. The surface reaction rate is

$$\dot{s}_i = k_{f\ si} \left(c_{i,f} - c_{i,s} \right)$$

TABLE 3 | Model parameters for the simulations of the dynamic experiments with the packed bed reactor model.

Reactor ID (m)	0.006
Bed length (m)	0.006
Bed porosity (-)	0.4
$F_{cat/geo}$	$1.03\ 10^5$
Inlet gas velocity—step 1 (m/s)	0.040 (@25°C)
Inlet gas velocity—step 2 (m/s)	0.154 (@25°C)
Inlet gas velocity—step 3 (m/s)	0.065 (@25°C)

TABLE 4 | Characterization results of the bifunctional catalyst Pt-O-NOMP [22].

Specific surface area, S_{BET} ($m^2\ g^{-1}$)	415
Average particle size (m)	$303\ 10^{-6}$
Pore width (m)	$4.98\ 10^{-9}$
Pore volume ($cm^3\ g^{-1}$)	0.78
N content ($mmol\ g^{-1}$)	1.6
Pt content (wt.%)	3.4
Pt metal dispersion (%)	34.3

and

$$k_{f\ si} = \frac{Sh_{fs} D_i}{d_p}$$

where k_{fsi} is the fluid-solid mass transfer coefficient for species i, $c_{i,f}$ is the fluid phase concentration of species i, $c_{i,s}$ is the particle surface concentration of species i, Sh_{fs} is the Sherwood number for fluid/solid mass transfer, D_i the effective diffusion for species i, and d_p is the particle size.

For the simulations of the two-step CO_2 capture and formation of methanol, the DETCHEM^{PBR_TRANSIENT} simulation package was used and the model parameters were modified to represent the experimental reactor setup. The model parameters are given in Table 3.

3 | Results and Discussion

The detailed characterization of the material is described and discussed in detail elsewhere [22]. For brevity, we report here the basic characterization that has been used to calculate the input parameters for the simulations (Table 4).

3.1 | CO_2 Capture

The adsorption of CO_2 is primarily affected by the amine density, the pore structure and morphology of the material as well as

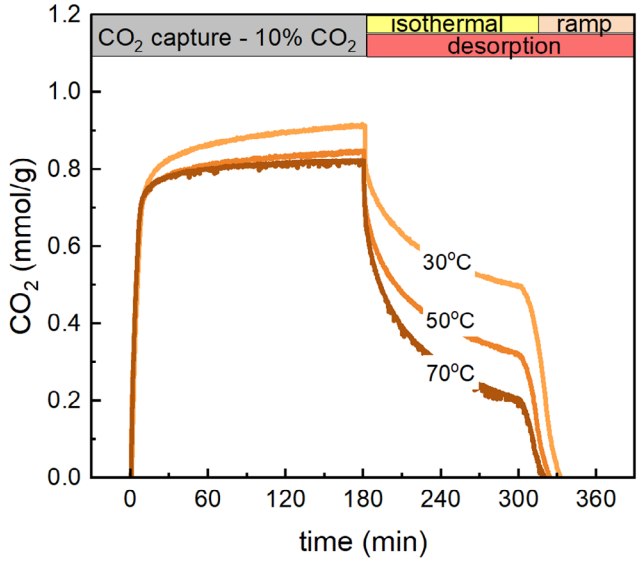

FIGURE 1 | CO_2 uptake profiles measured by TGA at different temperatures. The desorption takes place isothermally at the same temperature as the adsorption and then the temperature is linearly increased to 90°C with 3 K min^{-1}. Adsorption: 10 vol.% CO_2, 100 mL min^{-1}. Desorption: 100% N_2, 150 mL min^{-1}.

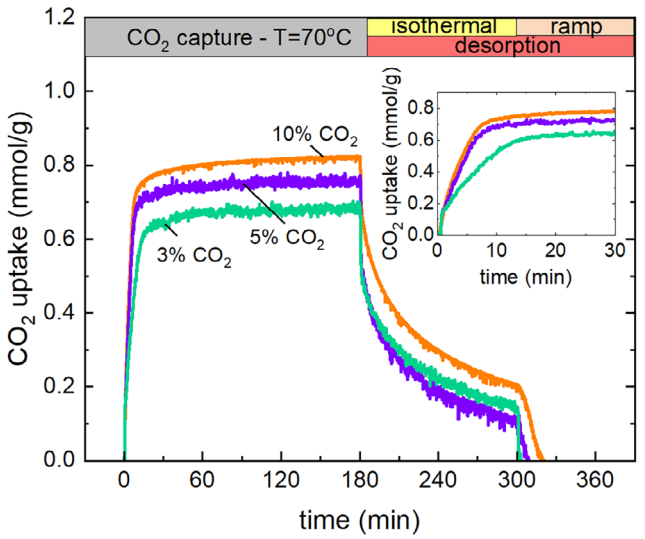

FIGURE 2 | CO_2 uptake profiles measured by TGA at different CO_2 inlet concentration. The desorption takes place isothermally at the same temperature as the adsorption and then the temperature is linearly increased to 90°C with 3 K min^{-1}. Adsorption: 70°C, 100 mL min^{-1}. Desorption: 100% N_2, 150 mL min^{-1}.

the CO_2 concentration in the feed and the temperature. The effect of temperature on CO_2 capture over the bifunctional catalyst is shown in Figure 1. The CO_2 adsorption capacity was determined using a 10 vol.% CO_2/N_2 mixture at ambient pressure to simulate stream composition in post-combustion systems [27]. The thermogravimetric curve during the CO_2 capture step shows the typical profile of a gas-solid reaction, that is, a fast increase in the sample mass at the beginning of the experiment due to reaction of the gas with the easily accessible capture sites (reaction-controlled regime) followed by slow increase of sample mass due to diffusion limited rate of reaction [28]. As shown in Figure 1, the CO_2 adsorption behavior on Pt/O-NOMP material was investigated through three distinct stages at varying temperatures. In the first stage (CO_2 capture), the sample mass increased upon CO_2 exposure until saturation of the capture sites and reaching the equilibrium CO_2 uptake, q_e. The equilibrium adsorption capacity (q_e) exhibited an inverse correlation with temperature, suggesting the exothermic nature of -NH_2 mediated CO_2 adsorption process. Pt/O-NOMP shows promising performance even at 70°C, reaching a total CO_2 uptake of 0.728 mmol g^{-1}, with 0.204 mmol g^{-1} CO_2 remaining irreversibly adsorbed after purging at 70°C (Table 1) thus achieving an amine efficiency as high as 45.5%. Since two amine sites are required for the capture of one CO_2 molecule, the maximum amine efficiency that can be theoretically achieved is 50% [18, 29]. During the second stage, the gas flow was switched to pure N_2 to purge the system. This resulted in the desorption of physisorbed and weakly chemisorbed CO_2, while a fraction remained strongly adsorbed (q_{chem}). In the final regeneration stage, heating to 90°C induced further weight loss, indicating complete CO_2 desorption and concomitant recovery of amine groups in the catalyst framework.

The effect of CO_2 content in the feed was also investigated, since it affects not only the reaction rate but also the equilibrium CO_2 uptake. Additionally, the equilibrium CO_2 uptake is decreased at lower CO_2 content because of the milder driving force of diffusion within the pore structure [30]. Decreasing the CO_2 content resulted in a decrease in the initial rate of adsorption as shown in the inset graph of Figure 2 resulting in a delay in the time of the transition from the surface reaction-controlled regime to the diffusion-controlled regime from ca. 7 min under 10% CO_2 to ca. 14 min under 3% CO_2. The initial slope of the CO_2 uptake (onset graph of Figure 2) is almost identical for the inlet concentrations of 5% and 10%, indicating a zero order upon CO_2, whereas at 3% CO_2 in the feed the capture rate is severely limited. In literature, the effect of the CO_2 concentration is investigated in terms of the effect on the capture capacity rather than the effect on the capture rate [31–34]. Despite our experimental evidence that the order of the reaction might be lower than 1, in the kinetic model developed here, we assumed that the order of the reaction follows the stoichiometry, that is, $n = 1$.

For better description of methanol formation under dynamic conditions, accurate model prediction of the CO_2 desorption profile is of utmost importance. The TGA data shown in Figure 1, depict the sample mass increase due to CO_2 capture upon exposure to the CO_2 inlet flow. The capture corresponds to the slight reduction of the outlet molar fraction of CO_2 that exits the reactor, which returns to the value of the inlet concentration once the sample has reached the equilibrium CO_2 uptake. During the desorption phase of the TGA experiment, the inlet CO_2 concentration is set to zero at the temperature of the adsorption step, therefore the CO_2 that exits the reactor corresponds to the desorption of physisorbed or weakly bond CO_2. Once this step is equilibrated, the temperature programmed desorption step takes place, which corresponds to the steeper decrease of the sample mass and accordingly the CO_2 uptake. In terms of the outlet CO_2 content, this decrease in the CO_2 uptake during the temperature-programmed step results in a peak in the CO_2 outlet mole fraction as shown in Figure 3. The CO_2 mole fraction profile in Figure 3 was not measured by an analytic device at the exit of the reactor,

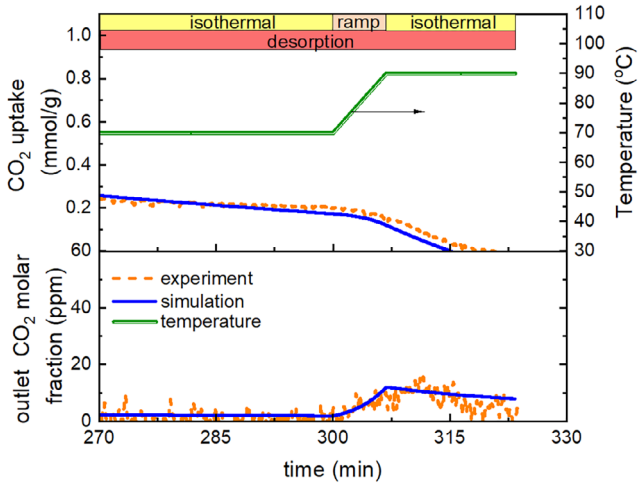

FIGURE 3 | TGA data of CO_2 desorption and the calculated outlet molar fraction of CO_2 in comparison to simulation. Adsorption: 10 vol.% CO_2, 70°C, 100 mL min^{-1}. Desorption: 100% N_2, 150 mL min^{-1}.

TABLE 5 | Kinetic coefficients of CO_2 capture reactions ("s" refers to amine sites).

Reaction	A (cm, mol, s)	B	E_α (kJ mol^{-1})
$CO_2 + 2s \rightarrow CO_2(ads) + s$	$5\,10^{13}$	−5.0	6.3
$CO_2(ads) + s \rightarrow CO_2(g) + 2s$	$2\,10^{10}$	0.01	91.5

but rather calculated considering that the mass change occurs exclusively due to CO_2 capture or release. The advantage in this case is that the profiles are free from effects of dead volume and flow hysteresis, but since the "theoretical" outlet CO_2 is very sensitive to slight fluctuations in sample mass, the profiles can be noisy. The kinetic model of CO_2 capture was developed in order to minimize the deviation of the temperature-programmed desorption profile as well as the chemisorbed CO_2 uptake, which in the form of ammonium carbamate is the critical intermediate for the formation of methanol under hydrogenation conditions [6, 8]. The kinetic coefficients of the CO_2 capture model are reported in Table 5. Kinetic investigation over PEI-modified nanocarbons reported an experimentally derived apparent activation energy of 13.3 and 22.6 kJ mol^{-1} based on isothermal adsorption experiments [35]. However, it is often the case that the experimentally observed rates are affected by diffusion limitations, thus, affecting the apparent activation energy determination [36]. The values reported here cannot be directly compared to apparent activation energies, since here coefficients refer to the global reaction R4 and are reported for the forward and the backward reaction separately. Activation energies derived from first principles for the elementary step processes report values in the range of 92–102 kJ mol^{-1} or even higher [34, 37].

The simulated temperature-programmed desorption profile in terms of CO_2 uptake and CO_2 outlet mole fraction after adsorption at 70°C is shown in Figure 3. The position and the slope of the desorption peak are well described and the peak height is

TABLE 6 | Capture capacity at different temperatures under 10% CO_2.

q_{chem} (mg g^{-1})			
50°C		70°C	
exp.	sim.	exp.	sim.
$0.72\,10^{-2}$	$1.21\,10^{-2}$	$0.46\,10^{-2}$	$0.69\,10^{-2}$

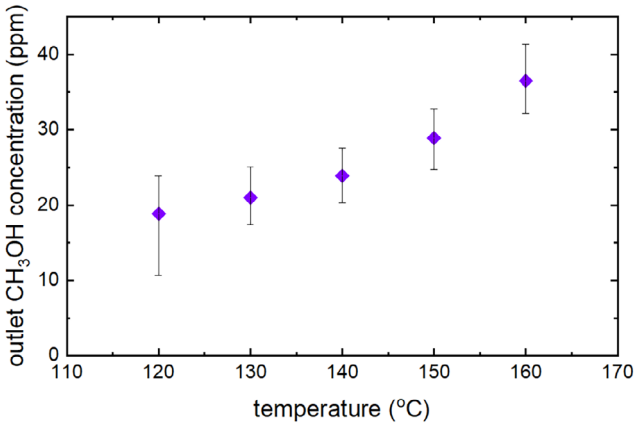

FIGURE 4 | Outlet mole fraction of methanol under steady state CO_2 hydrogenation experiments over the bifunctional catalyst at varying temperature (H_2:CO_2= 3, GHSV=34,000 h^{-1}).

within the same range leading to a good agreement of the TGA profiles. The peak integration of the flow profiles determines the simulated chemisorbed uptake, q_{chem}, which is well within the range of the experimental values (Table 6).

3.2 | Steady-State Methanol Formation Kinetics

The integrated process described here is not intended to replace the conventional CO_2 hydrogenation to methanol process, but rather to efficiently convert captured CO_2 to a chemical energy carrier. In that sense, the process involves two stages, where first the CO_2 capture takes place, and during the second stage, the surface species are converted to methanol in the presence of hydrogen. However, in order to extract information on the kinetics of the methanol formation over the bifunctional catalyst while cofeeding CO_2 and H_2, it was required to run steady state experiments at various temperatures. The steady-state outlet methanol concentration as a function of temperature is given in Figure 4. The outlet molar fraction of methanol at the temperature of 120°C is 19 ppm and after increasing the temperature to 160°C, the methanol outlet molar fraction increased up to 36 ppm. The low conversion of H_2 achieved at these experiments serves the purpose of determining kinetic information. In addition, thermodynamic limitations can also be excluded because H_2 is present in the gas phase during the hydrogenation step, while CO_2 is chemically bound to the surface as amide. Therefore, all molecules bound to sites at the metal-amine interface can be converted to methanol.

The Arrhenius plot for the methanol formation kinetic experiments is shown in Figure 5. Through the linear fitting of the

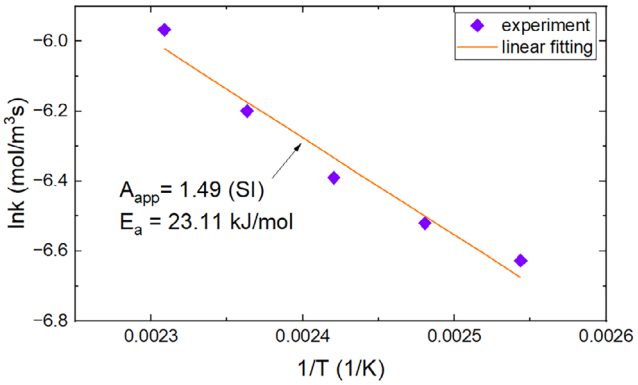

FIGURE 5 | Arrhenius plot of steady state CO_2 hydrogenation over the bifunctional catalyst Pt/O-NOMP at varying temperature (H_2: CO_2 = 3, GHSV = 34,000 h^{-1}).

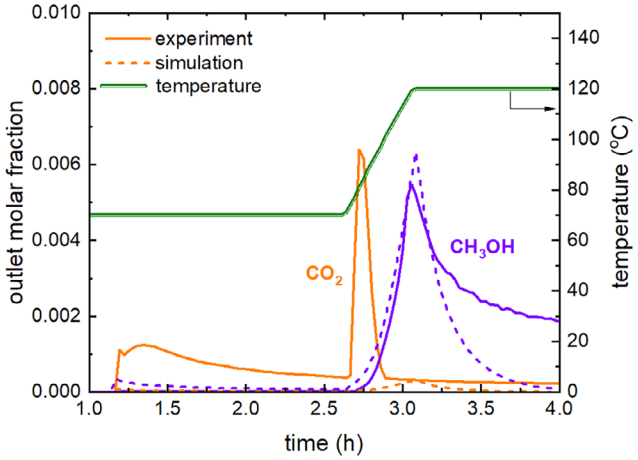

FIGURE 6 | Dynamic experiment of methanol formation over the bifunctional catalyst under sequential steps of CO_2 capture and hydrogenation. Adsorption: 10% CO_2 in He, 70°C, Hydrogenation: 30% H_2 in He, T = 70–90°C, ramp 3 K min^{-1}.

experimental data points an apparent activation energy of 23.11 kJ mol^{-1} was calculated. Even though the apparent activation energy is low, the overall kinetics are slow, due to the low apparent preexponential factor and the low temperature. The overall process is probably limited by the kinetics of the CO_2 capture; therefore, the two-step process provides the flexibility for process optimization.

3.3 | Methanol Formation Under Dynamic Operation

The kinetic model for the CO_2 capture as well as the conversion to methanol was validated against experimental data obtained under dynamic conditions where methanol is formed in two steps. At the first step, CO_2 is captured at 70°C under 10% CO_2 and after a purging step, the hydrogenation step takes place first isothermal at 70°C and then at linearly increasing temperature to 120°C. After reaching the CO_2 sorption equilibrium, the experimentally determined outlet molar fractions are shown in Figure 6. N_2 was used to purge the system keeping the temperature at 70°C, to remove the weakly and physisorbed CO_2 from the sorbent/catalysts preventing potential blocking of the amine groups. The hydrogenation was carried out in 30 vol.% H_2 in He, during the temperature increase to 120°C. Only CO_2, CH_3OH, and H_2O were detected during the hydrogenation step, whereas additional side products (e.g., CH_4, CO, and C_2 oxygenates) were not detected, indicating 100% selectivity for the conversion of CO_2 to methanol. The temperature of 70°C was selected as the reference temperature of the CO_2 capture step in order to ensure high capture capacity but also minimize the loss of the captured CO_2 in the form of gaseous CO_2 during the hydrogenation step.

The simulation of the dynamic experiment and its comparison to the experimental data was used as a validation of the model and has been executed using the kinetic information extracted from the previous sections. The simulation temporal profiles of CO_2 and methanol are shown in Figure 6. After 1 h of experiment, the flow is switched and the CO_2 mole fraction starts decreasing. The delay in this case in returning to the nominal signal of CO_2 can be attributed not only to desorbed CO_2 due to the current conditions, but also to possible diffusion limitations, which are also considered in the model. Therefore, in case external diffusion is limiting the rate during the experiment, the model should also be able to predict its performance. Once hydrogen is introduced into the system, a wide peak of CO_2 appears in the experimental profile, which is attributed to physisorbed or weakly bonded CO_2, which does not contribute to the conversion to methanol. This trend is not accurately described by the model because physisorption is not considered in the model reactions; therefore, the desorption of these species would not be present in the simulated temporal CO_2 profile. The amount of CO_2 that is present in this purging stage corresponds to the equilibration of the adsorption/desorption reaction to the current inlet CO_2 concentration. In addition, slight distortions of the MS signals caused by valve changing during the experiment do not allow a valid comparison to the simulation at this stage. This phenomenon was eliminated during the TGA experiments because in that case the mass of the sample is measured, instead of the exit gas.

The simulation of the temperature-programmed hydrogenation step reveals peaks of both methanol and CO_2, starting to form at the same time. This indicates that the formation of methanol is limited by the desorption of CO_2, so once CO_2 starts desorbing, part of it is converted to methanol. In the experiment, the CO_2 peak appears before the methanol peak, indicating that the localization of the captured CO_2 within the material pores and the proximity to the metal sites restricts the utilization of the captured CO_2. The mean-field approximation applied for the model simulation considers that the surface is uniform and that the active sites are evenly distributed, therefore such effects of localization of adsorbed species cannot be predicted [38]. The sequential order of the experimental peaks of CO_2 and methanol could be explained by a possible kinetic limitation of the methanol formation reaction that requires slightly higher temperature to occur than the desorption of CO_2 reaction.

The methanol formation kinetics is well described by the model with respect to the initial slope of the peak and the temperature dependency as well as the peak height, factors crucial for the predictive performance of the model at possible operation scenarios and optimized experimental material testing protocols.

TABLE 7 | Parameters investigated in the simulation study.

Parameter	Range
Desorption flow rate (mL min^{-1})	44, 50, 55
Adsorption temperature (°C)	50, 70, 90
Isothermal operation temperature (°C)	70, 80, 90, 100

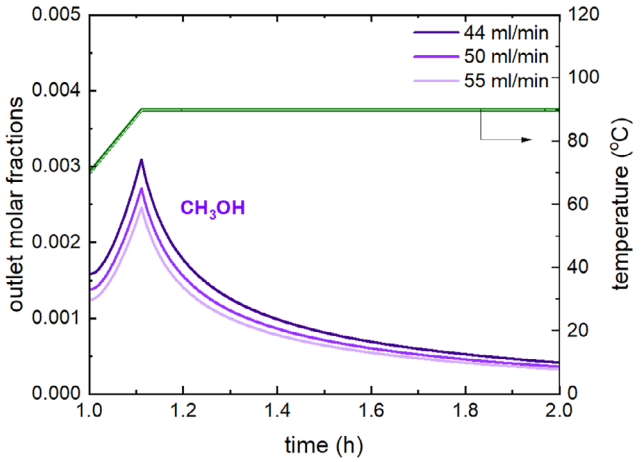

FIGURE 7 | Effect of hydrogenation flow rate on the formation of methanol. Adsorption: 10% CO_2 in He, 70°C, Hydrogenation: 30% H_2 in He, $T = 70–90$°C, ramp 3 K min^{-1}.

The optimization of the experimental testing protocol is realized by conducting a parametric simulation study employing the developed model. For the parametric study, the conditions of the dynamic validation experiment are set as reference conditions. The parameters modified are summarized in Table 7.

The effect of the flow rate during the hydrogenation stage on the methanol formation peak is shown in Figure 7. The increased flow rate resulted in a decrease in the methanol peak, because of the lower residence time of hydrogen. Additionally, a decrease in the methanol molar fraction is also expected because of the increase in the total flow, even if the reaction rate would not be affected. However, the increase in the flow rate significantly reduces the tail of the methanol peak, enabling a reduction of the hydrogenation duration to make the testing protocol more time efficient.

The adsorption temperature affects the testing protocol on the one side via the amount of captured CO_2 and on the other side via the time required for the heating of the reactor from the adsorption temperature to the hydrogenation temperature. As shown in Figure 8, the methanol peak position is shifted to lower time when the adsorption temperature is higher, because less time is required to achieve the hydrogenation temperature. During the heating of the reactor, the sample is exposed to the hydrogenation gas, therefore the formation of methanol may start already during this stage. However, when the temperature at the gas switch is higher, the rate of methanol formation is higher, leading to the peak becoming sharper.

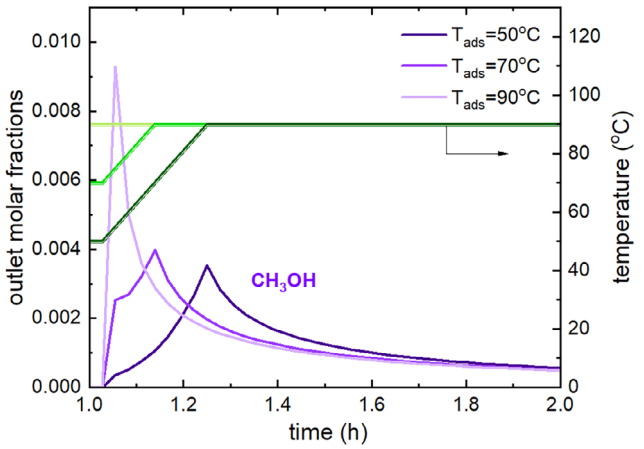

FIGURE 8 | Hydrogenation step during Temperature Swing Operation. Effect of adsorption temperature. Adsorption: 10% CO_2 in He, Hydrogenation: 30% H_2 in He, $T = 90$°C, ramp 3 K min^{-1}.

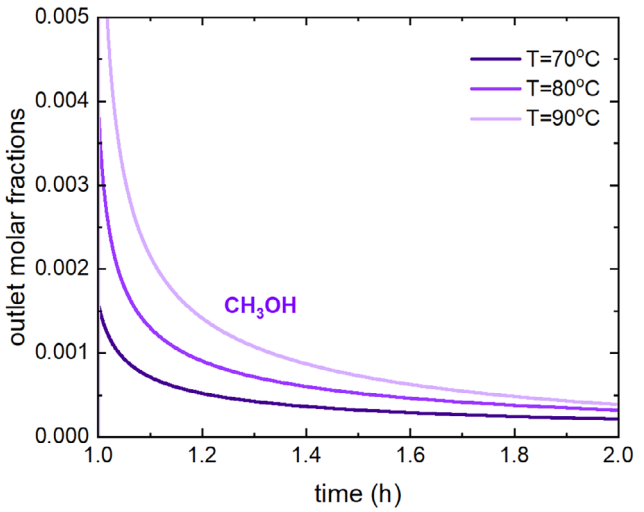

FIGURE 9 | Hydrogenation step of isothermal operation cycle. Adsorption: 10% CO_2 in He. Hydrogenation: 30% H_2 in He.

The behavior of the methanol formation was also studied in isothermal mode, where the reactor is kept under constant temperature and the gas is switched from the adsorption gas to the hydrogenation gas periodically. This testing protocol offers the advantage of simplifying of the experimental procedure and eliminating the heating times. In Figure 9, it is shown that since there is no intermediate heating stage, the methanol peak starts before the CO_2 goes to zero, which leads to a steep methanol peak. Additionally, the higher hydrogenation temperature increases the methanol formation rate.

Even though the experimental conditions affect the methanol formation rate, the peak is characterized by a long tail, which restricts the duration of the experimental procedure. The tail indicates a low desorption rate probably limited by diffusion. The optimization of the material properties with respect to pore structure would eliminate the rate suppression due to slow diffusion of

the methanol molecules. Additional optimization strategy would be to vary the ratio of metal loading and the dispersion, in order to ensure that the CO_2 captured is in proximity to the metal sites and will be efficiently converted to methanol.

4 | Conclusion

This work reports the development of a kinetic model for the dynamic CO_2 capture and conversion to methanol over a bifunctional Pt/amine-based material. CO_2 capture kinetics were derived from TGA experiments under various conditions, while the conversion of methanol kinetics was evaluated under steady state conditions. The model predictions under transient simulations of the dynamic experiment, where CO_2 capture and hydrogenation are conducted at sequential steps, fairly predicted the methanol formation in a temperature ramping mode, indicating the accurate capture of the reaction kinetics. The simulation predicts desorption of unreacted CO_2 in the hydrogenation step only in small concentrations compared to methanol, which is not validated by experiments, probably due to effects of local proximity of the amine sites to the Pt sites, which cannot be distinguished under the mean field approximation. The parametric investigation of the dynamic experiment conditions showed that the isothermal cycles under periodically switching gases offers a good compromise between lower CO_2 capture capacity and higher methanol formation rates in combination with the time-efficient experimental protocol. Further investigation on the material design with regard to methanol desorption optimization and even higher efficiency toward the utilization of the metal sites will accordingly facilitate the development of the process. In addition, a systematic investigation of the influence of components contained in flue gases, such as H_2O and SO_2, on the mechanism and the overall performance will bring the concept closer to application.

Acknowledgments

The work was supported by the Deutsche Forschungsgemeinschaft (DFG), the German Research Foundation, within the priority program SPP 2080 "Catalysts and Reactors under Dynamic Conditions for Energy Storage and Conversion" (project no. 406474220, DE 659/13-2, GL 290/12-2, JE 260/13-2). The authors thank omegadot software & consulting GmbH, Limburgerhof, Germany, for the cost-free academic license of DETCHEM.

Open access funding enabled and organized by Projekt DEAL.

Conflicts of Interest

The authors declare no conflict of interest.

Data Availability Statement

The data that support the findings of this study are available from the corresponding author upon reasonable request.

References

1. E. Alper and O. Yuksel Orhan, "CO2 Utilization: Developments in Conversion Processes," *Petroleum* 1 (2017): 109–126, https://doi.org/10.1016/j.petlm.2016.11.003.

2. S. G. Jadhav, P. D. Vaidya, B. M. Bhanage, and J. B. Joshi, "Catalytic Carbon Dioxide Hydrogenation to Methanol: a Review of Recent Studies," *Chemical Engineering Research and Design* 92 (2014): 2557–2567, https://doi.org/10.1016/j.cherd.2014.03.005.

3. V. Dieterich, A. Buttler, A. Hanel, H. Spliethoff, and S. Fendt, "Power-To-Liquid via Synthesis of Methanol, DME or Fischer–Tropsch-Fuels: a Review," *Energy & Environmental Science* 13 (2020): 3207–3252, https://doi.org/10.1039/d0ee01187h.

4. R. Sen, C. J. Koch, V. Galvan, N. Entesari, A. Goeppert, and G. K. S. Prakash, "Glycol Assisted Efficient Conversion of CO2 Captured From Air to Methanol With a Heterogeneous Cu/ZnO/Al2O3 Catalyst," *Journal of CO2 Utilization* 54 (2021): 101762, https://doi.org/10.1016/j.jcou.2021.101762.

5. J. Zhong, X. Yang, Z. Wu, B. Liang, Y. Huang, and T. Zhang, "State of the Art and Perspectives in Heterogeneous Catalysis of CO2 Hydrogenation to Methanol," *Chemical Society Reviews* 49 (2020): 1385–1413, https://doi.org/10.1039/c9cs00614a.

6. J. Kothandaraman, A. Goeppert, M. Czaun, G. A. Olah, and G. K. S. Prakash, "Conversion of CO2 From Air Into Methanol Using a Polyamine and a Homogeneous Ruthenium Catalyst," *Journal of the American Chemical Society* 138 (2016): 778–781, https://doi.org/10.1021/jacs.5b12354.

7. N. M. Rezayee, C. A. Huff, and M. S. Sanford, "Tandem Amine and Ruthenium-Catalyzed Hydrogenation of CO2 to Methanol," *Journal of the American Chemical Society* 137 (2015): 1028–1031, https://doi.org/10.1021/ja511329m.

8. L. Jiang, W. Liu, R. Q. Wang, et al., "Sorption Direct Air Capture With CO2 Utilization," *Progress in Energy and Combustion Science* 2022 (2023): 101069, https://doi.org/10.1016/j.pecs.2022.101069.

9. Z. Yang, C. Yue, W. Pang, et al., "Amine-Mediated Carbon Dioxide Capture and In-Situ Conversion," *Chemical Engineering Science* 317 (2025): 122104, https://doi.org/10.1016/j.ces.2025.122104.

10. W. W. McNeary, N. C. Ellebracht, M. L. Jue, et al., "Application of Solid-Supported Amines for Thermocatalytic Reactive CO2 Capture," *ACS Omega* 10 (2025): 2364–2371, https://doi.org/10.1021/acsomega.4c10049.

11. S. Kar, A. Goeppert, and G. K. S. Prakash, "Combined CO2 Capture and Hydrogenation to Methanol: Amine Immobilization Enables Easy Recycling of Active Elements," *Chemsuschem* 12 (2019): 3172–3177, https://doi.org/10.1002/cssc.201900324.

12. S. Kar, R. Sen, J. Kothandaraman, et al., "Mechanistic Insights Into Ruthenium-Pincer-Catalyzed Amine-Assisted Homogeneous Hydrogenation of CO2to Methanol," *Journal of the American Chemical Society* 141 (2019): 3160–3170, https://doi.org/10.1021/jacs.8b12763.

13. S. T. Bai, C. Zhou, X. Wu, R. Sun, and B. Sels, "Suppressing Dormant Ru States in the Presence of Conventional Metal Oxides Promotes the Ru-MACHO-BH-Catalyzed Integration of CO2Capture and Hydrogenation to Methanol," *ACS Catalysis* 11 (2021): 12682–12691, https://doi.org/10.1021/acscatal.1c02638.

14. M. Everett and D. F. Wass, "Highly Productive CO 2 Hydrogenation to Methanol—A Tandem Catalytic Approach via Amide Intermediates," *Chemical Communications* 53 (2017): 9502–9504, https://doi.org/10.1039/c7cc04613h.

15. R. Kumar, T. Mandal, A. Bhattacherya, M. K. Pandey, J. K. Bera, and J. Choudhury, "Hyper-Cross-Linked Polymer-Based Self-Supported Reusable Ru-NHC Catalyst for Amine-Assisted Hydrogenation of CO2 to Methanol," *ACS Catalysis* 14 (2024): 13236–13245, https://doi.org/10.1021/acscatal.4c02513.

16. J. Pazdera, E. Berger, J. A. Lercher, and A. Jentys, "Conversion of CO2 to Methanol Over Bifunctional Basic-Metallic Catalysts," *Catalysis Communications* 159 (2021): 106347, https://doi.org/10.1016/j.catcom.2021.106347.

17. J. Pazdera, D. Issayeva, J. Titus, R. Gläser, O. Deutschmann, and A. Jentys, "Impact of the Local Environment of Amines on the Activity for CO2 Hydrogenation over Bifunctional Basic—Metallic Catalysts,"

Chemcatchem 14 (2022): e202200620 (1-10), https://doi.org/10.1002/cctc.202200620.

18. K. Basaran, U. Topcubasi, and T. Davran-Candan, "Theoretical Investigation of CO2 Adsorption Mechanism Over Amine-Functionalized Mesoporous Silica," *Journal of CO2 Utilization* 47 (2021): 101492–101508, https://doi.org/10.1016/j.jcou.2021.101492.

19. Y. Meng, D. Gu, F. Zhang, et al., "Ordered Mesoporous Polymers and Homologous Carbon Frameworks: Amphiphilic Surfactant Templating and Direct Transformation," *Angewandte Chemie International Edition* 44 (2005): 7053–7059, https://doi.org/10.1002/anie.200501561.

20. X. Cui, Q. Yang, Y. Xiong, Z. Bao, H. Xing, and S. Dai, "Preparation of Ordered N-Doped Mesoporous Carbon Materials via a Polymer–Ionic Liquid Assembly," *Chemical Communications* 53 (2017): 4915–4918, https://doi.org/10.1039/c7cc01000a.

21. W. Zhu, Y. Wang, F. Yao, et al., "One-Pot Synthesis of N-Doped Petroleum Coke-Based Microporous Carbon for High-Performance CO2 Adsorption and Supercapacitors," *Journal of Environmental Sciences* 139 (2024): 93–104, https://doi.org/10.1016/j.jes.2023.02.008.

22. H. Xu, S. Bartling, E. V. Kondratenko, and A. Jentys, "One-Step Synthesis of Amine-Doped Ordered Mesoporous Polymers and Application to Hydrogenation of CO2 to Methanol Dynamic Reaction Conditions," *Chemcatchem* (2025): e01297, https://doi.org/10.1002/cctc.202501297.

23. S. A. Didas, M. A. Sakwa-Novak, G. S. Foo, C. Sievers, and C. W. Jones, "Effect of Amine Surface Coverage on the Co-Adsorption of CO2 and Water: Spectral Deconvolution of Adsorbed Species," *Journal of Physical Chemistry Letters* 5 (2014): 4194–4200, https://doi.org/10.1021/jz502032c.

24. M. W. Hahn, J. Jelic, E. Berger, K. Reuter, A. Jentys, and J. A. Lercher, "Role of Amine Functionality for CO2 Chemisorption on Silica," *Journal of Physical Chemistry B* 8 (2016): 1988–1995, https://doi.org/10.1021/acs.jpcb.5b10012.

25. N. N. Avgul, A. V. Kiselev, and I. A. Lygina, "The Adsorption Energies of CO2, SO2, (CH3)2CO and (C2H5)2O on Graphite," *Otdelenie Khimieheskikh Nauk* 2 (1961): 24–30.

26. R. Chacko, K. Keller, S. Tischer, et al., "Automating the Optimization of Catalytic Reaction Mechanism Parameters Using Basin-Hopping: a Proof of Concept," *Journal of Physical Chemistry C* 127 (2023): 7628–7639, https://doi.org/10.1021/acs.jpcc.2c08179.

27. I. Ghiat and T. Al-Ansari, "A Review of Carbon Capture and Utilisation as A CO2abatement Opportunity within the EWF Nexus," *Journal of CO2 Utilization* 2020 (2021): 101432, https://doi.org/10.1016/j.jcou.2020.101432.

28. S. D. Angeli, C. S. Martavaltzi, and A. A. Lemonidou, "Development of a Novel-Synthesized Ca-Based CO2 Sorbent for Multicycle Operation: Parametric Study of Sorption," *Fuel* 127 (2014): 62–69, https://doi.org/10.1016/j.fuel.2013.10.046.

29. T. C. Dos Santos, S. Bourrelly, P. L. Llewellyn, J. W. D. M. Carneiro, and C. M. Ronconi, "Adsorption of CO2 on Amine-Functionalised MCM-41: Experimental and Theoretical Studies," *Physical Chemistry Chemical Physics* 17 (2015): 11095–11102, https://doi.org/10.1039/c5cp00581g.

30. Y. Zhai and S. S. C. Chuang, "The Nature of Adsorbed Carbon Dioxide on Immobilized Amines during Carbon Dioxide Capture From Air and Simulated Flue Gas," *Energy Technology* 5 (2017): 510–519, https://doi.org/10.1002/ente.201600685.

31. F. Liu, K. Huang, C. J. Yoo, et al., "Facilely Synthesized Meso-Macroporous Polymer as Support of Poly(Ethyleneimine) for Highly Efficient and Selective Capture of CO2," *Chemical Engineering Journal* 314 (2017): 466–476, https://doi.org/10.1016/j.cej.2016.12.004.

32. X. E. Hu, L. Liu, X. Luo, et al., "A Review of N-Functionalized Solid Adsorbents for Post-Combustion CO2 Capture," *Applied Energy* 260 (2020): 114244, https://doi.org/10.1016/j.apenergy.2019.114244.

33. A. Heydari-Gorji and A. Sayari, "CO2 Capture on Polyethylenimine-Impregnated Hydrophobic Mesoporous Silica: Experimental and Kinetic Modeling," *Chemical Engineering Journal* 173 (2011): 72–79, https://doi.org/10.1016/j.cej.2011.07.038.

34. K. Li, J. D. Kress, and D. S. Mebane, "The Mechanism of CO2 Adsorption under Dry and Humid Conditions in Mesoporous Silica-Supported Amine Sorbents," *Journal of Physical Chemistry C* 120 (2016): 23683–23691, https://doi.org/10.1021/acs.jpcc.6b08808.

35. E. Andreoli, L. Cullum, and A. R. Barron, "Carbon Dioxide Absorption by Polyethylenimine-Functionalized Nanocarbons: a Kinetic Study," *Industrial & Engineering Chemistry Research* 54 (2015): 878–889, https://doi.org/10.1021/ie504277s.

36. Q. Liu, J. Shi, S. Zheng, M. Tao, Y. He, and Y. Shi, "Kinetics Studies of CO2 Adsorption/Desorption on Amine-Functionalized Multiwalled Carbon Nanotubes," *Industrial & Engineering Chemistry Research* 53 (2014): 11677–11683, https://doi.org/10.1021/ie502009n.

37. R. Ben Said, J. M. Kolle, K. Essalah, B. Tangour, and A. Sayari, "A Unified Approach to CO 2 –Amine Reaction Mechanisms," *ACS Omega* 5 (2020): 26125–26133, https://doi.org/10.1021/acsomega.0c03727.

38. L. Kunz, L. Maier, S. Tischer, and O. Deutschmann, "Modeling the Rate of Heterogeneous Reactions," in *Modeling and Simulation of Heterogeneous Catalytic Reactions* (2011): 113–148, https://doi.org/10.1002/9783527639878.ch4.